On a Universal Model for the Prediction of the Daily Global Solar Radiation

S. Kaplanis[a,*], Jatin Kumar[a], E. Kaplani[a,b]

[a]Mechanical Engineering Department, Technological Educational Institute of Western Greece, Meg. Alexandrou 1, Patra 26334, Greece
[b]School of Mathematics, University of East Anglia, Norwich NR4 7TJ, UK

*Corresponding author. Email address: kaplanis@teiwest.gr

Abstract

A model to predict the mean expected daily global solar radiation, H(n) on a day n, at a site with latitude φ is proposed. The model is based on two cosine functions. A regression analysis taking into account the mean measured values $H_{m.meas}(n)$ obtained from SoDa database for 42 sites in the Northern Hemisphere resulted in a set of mathematical expressions of split form to predict H(n). The parameters of the two cosine model for $0^o<\varphi<23^o$ are obtained by regression analysis using a sum of 3-8 Gaussian functions, while for $23^o<\varphi<71^o$ the two cosine model parameters are expressed by a sum of exponential functions or the product of an exponential and a cosine function. The main equation of the model and the set of parametric expressions provide H(n) for any φ on Earth. Validation results of this model are provided along with the statistical estimators NMBE, NRMSE and t-statistic in comparison to the corresponding values from three databases of NASA, SoDa and the measured values from ground stations provided in Meteonorm.

Keywords: daily solar radiation, universal model, prediction

1. Introduction

The mean expected daily global solar radiation, H(n), on the horizontal plane in any place and on any day is an important factor and it may serve as data input in sizing projects related to solar collector and PV systems, as well as in meteorological projects. Therefore, solar radiation data collection is carefully managed and elaborated in any country. Many papers have been published outlining models which provide H(n) estimates. A couple of those models like the Iqbal model C and the ASHRAE [1-3] are semi- empirical and predict the beam and diffuse components of the global solar radiation in a site leading to an easy determination of the global daily values. Both are based on the theoretical and experimental estimation for the site concerned of certain physico-chemical quantities, optical properties of the solar light attenuation in the atmosphere, and simulation of the processes, even including multiple reflection processes between ground and sky. Other models starting from the Ångström-Prescott model [4] provide the H(n) values in any place based on various empirical expressions with the monthly mean daily fraction of possible sunshine hours [5-10]. An analytic approach is presented in the meteorological radiation models [11-12]. Another family of models correlates H(n) with ambient temperature, humidity, cloudiness, associated with the clearness index, and other meteorological parameters [13-16],

reaching up to models using artificial intelligence [17], while a third group of models provides expressions how to determine H(n) in a site with parameter the day of the year [18-23]. The regression analysis is the general tool to determine the values of the parameters through which these models are described. These values are valid for the region the model is tested, i.e. the latitude, and longitude and the microclimate, in general. The papers that have been published, as the abovementioned ones, present the mathematical expressions of the proposed models for the specific regions and provide an elaboration of the values of the parameters they depend on. The H(n) model expressions are grouped according to:

1. the day of the year, n, or some more complex expressions based on cyclic functions [20-22]. This model holds for $25^o<\varphi<60^o$.

$$H(n) = A + B\cos\left(\frac{2\pi}{365}n + C\right) \quad (1)$$

2. the actual sunshine hours on a day, S, over the theoretical daylight hours on that day, S_o based on the Ångström-Prescott model and its evolution with more complex functions [5-12]

$$\frac{H}{H_{ext}} = a + b\left(\frac{S}{S_o}\right) \quad (2)$$

where H_{ext} is the daily extraterrestial solar radiation on the horizontal plane [1].

3. several mixed-type expressions as below [13,22-23]

$$\frac{H}{H_{ext}} = a + \sum f\left(\frac{S}{S_o}\right) + \sum f'\left(\frac{S}{S_o}\right) + \cdots . + \sum f(T_{max}^m) + \sum f(RH) \quad (3)$$

where T_{max} is the maximum ambient temperature of the day and RH the relative humidity of the same day.

A, B, C, a, b etc. are parameters to be determined for any site by regression analysis. Based on the analysis carried out in the present work the least number of H(n) values required for a well-correlated fitting in a function as that in eq.(1) in order to obtain A,B,C is 6. Eq.(1) holds for latitudes around 23^o-60^o and provides H(n) values with a very good coefficient of determination, R^2, around 0.97-0.99 [24]. Mean monthly daily values of the global solar radiation may also be used for the need of the fitting as these values are close to the solar radiation value of the representative day of the month. Mean monthly daily values are provided by many databases like PVGIS, SoDa, Meteonorm, PVWatts, NREL, NASA, RETScreen [25-31]. Having determined H(n) the hourly global solar radiation for the site can be determined by the models outlined in [20,32-35]. Nevertheless, it is preferable that a universal model be set up to provide H(n) for any day at any site, without the need of any database, instead of performing regression analysis for each region to determine the model parameters.

2. Model Outline

The present investigation proposes a universal model, which predicts the global horizontal solar radiation H(n) as a function of the day (n) of the year, provided in eq.(4), along with a set of parametric mathematical expressions, which depend on the latitude φ. This is a two-cosine model applicable both in the Northern and Southern Hemispheres. A regression analysis was applied to the global solar radiation data from 42 sites from 0°N (Equator) to 71°N, as shown in Table 1, obtained from the SoDa database [26]. The mathematical expression for the proposed model is given below:

$$H(n) = A_1 + B_1 cos\left(C_1 \frac{2\pi}{365} n + D_1\right) + B_2 cos(C_2 \frac{2\pi}{365} n + D_2) \quad (4)$$

The regression analysis of the 12 mean monthly daily global horizontal solar radiation values taken from the SoDa database and carried out for each one of the 42 sites from eq.(4) gave the values of the unknown parameters A_1, B_1, B_2, C_1, C_2, D_1 and D_2.

Table 1: Sites used in regression analysis

S. No.	Site Name	Latitude, Longitude	S. No.	Site Name	Latitude, Longitude
1	Kasese, Uganda	0.1°N, 30.1°E	**22**	Boutilimit, Mauritania	17.55°N, 14.7°W
2	Kango, Gabon	0.17°N, 10.11°E	**23**	Dongola, North Sudan	19.1°N, 30.3°E
3	Kisangani, DR Congo	0.31°N, 25.11°E	**24**	Wadi, Maharashtra, India	21.15°N, 79.01°E
4	Gulu, Northern Uganda	2.45°N, 32.2°E	**25**	Wadi Halfa, North Sudan	21.5°N, 31.8°E
5	Batouri, Cameroon	4.43°N, 14.37°E	**26**	Aswan, Egypt	23.6°N, 32.5°E
6	Juba, South Sudan	4.5°N, 31.4°E	**27**	Asyut, Egypt	27.0°N, 31.0°E
7	Beledweyne, Somalia	4.73°N, 45.2°E	**28**	Ataqah, Egypt	30.0°N, 32.0°E
8	Jonglei, South Sudan	7.0°N, 32°E	**29**	Damascus, Syria	33.3°N, 36.3°E
9	New Brosankro, Ghana	7.03°N, 2.1°W	**30**	Alanya, Turkey	36.54°N, 32.0°E
10	Malakal, South Sudan	9.33°N, 31.39°E	**31**	Ankara, Turkey	39.6°N, 32.5°E
11	Bari, Somalia	9.5°N, 49.1°E	**32**	Black Sea	43.0°N, 32.0°E
12	Kamakwie, Sierra Leone	9.5°N, 12.23°W	**33**	Odessa, Ukraine	46.3°N, 30.4°E
13	Kadugli, South Sudan	11.0°N, 29.4°E	**34**	Kiev, Ukraine	50.2°N, 30.3°E
14	Ndjamena, Chad	12.0°N, 15.0°E	**35**	Suwalki, Poland	54.1°N, 22.6°E
15	Kedougou, Senegal	12.5°N, 12.18°W	**36**	Tver Oblast, Russia	57.0°N, 32.0°E
16	Gondar, Ethiopia	12.6°N, 37.47°E	**37**	St. Petersburg, Russia	59.6°N, 30.2°E
17	Bengaluru, India	12.97°N, 77.6°E	**38**	Jokioinen, Finland	60.49°N, 23.3°E
18	Wad Medani, North Sudan	14.24°N, 33.3°E	**39**	Jyväskylä, Finland	62.2°N, 25.4°E
19	Khartoum, North Sudan	15.36°N, 32.3°E	**40**	Umea, Sweden	63.5°N, 20.2°E
20	Tchirozérine, Niger	17.26°N, 7.83°E	**41**	Lulea, Sweden	65.3°N, 22.1°E
21	Hudeiba, UAE	17.34°N, 33.6°E	**42**	Nordkapp, Norway	71.0°N, 25.7°E

The fitting results of the model using the regression analysis in MATLAB, is shown in Figs. 1-4, for various sites, along with the coefficient of determination R^2, whose value for any latitude and

88 longitude was in the range 0.97-0.99, and the Root Mean Square Error (RMSE) whose value in
89 the range 0.09-0.34 $kWh \cdot m^{-2} \cdot d^{-1}$.

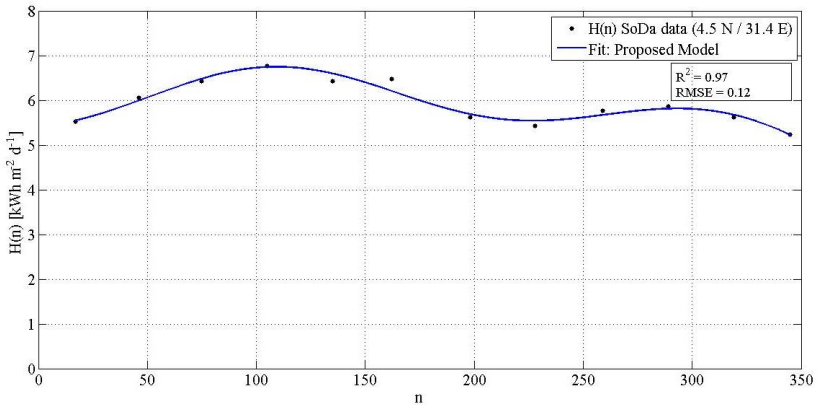

90

91 Fig. 1: SoDa mean monthly daily H(n) values and fitted curve by the proposed model for Juba,
92 Sudan (4.5°N, 31.4°E).

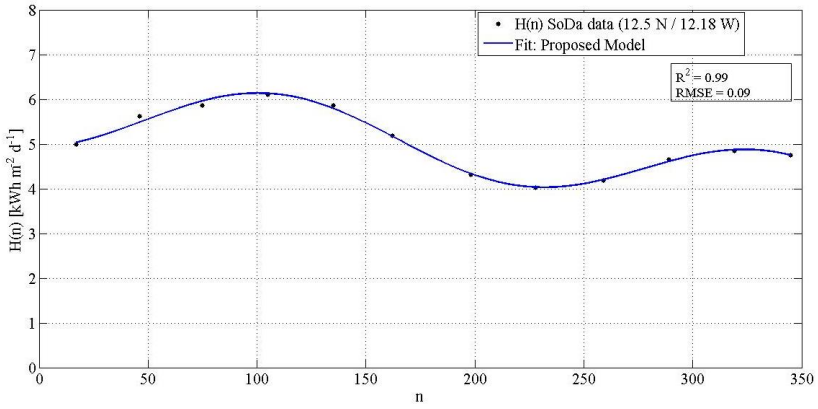

93
94 Fig. 2: As in Fig.1, but for Kedougou, Senegal (12.5°N, 12.18°W).
95

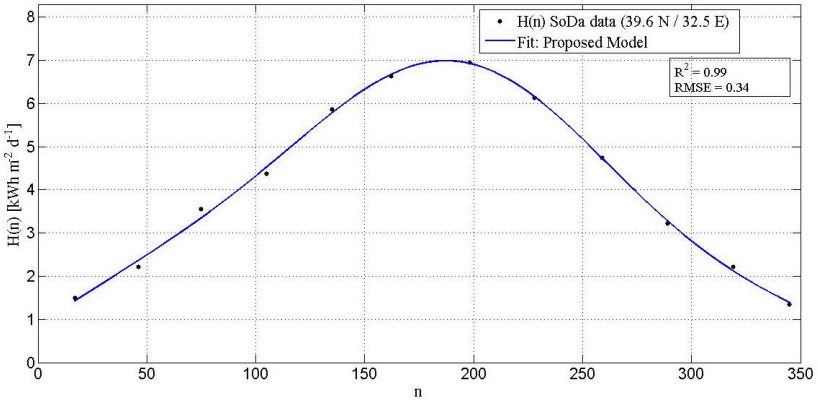

96
97 Fig. 3: As in Fig.1, but for Ankara (39.6°N, 32.5°E).

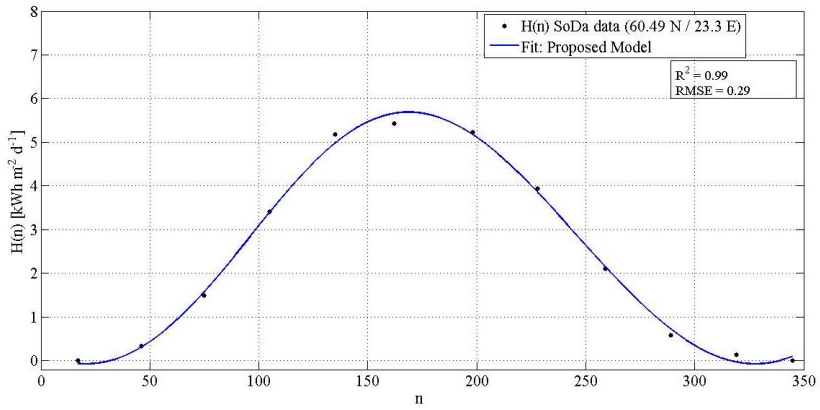

Fig. 4: As in Fig.1, but for Jokioinen, Finland (60.49°N, 23.3°E).

The methodology for determining the unknown parameters of the model in eq.(4) is presented in the following section.

3. Mathematical Expressions and Parameterization of the Model

As said, the regression analysis done for the H(n) data of the 42 sites provided a set of values for the seven parameters mentioned above. Each of those seven parameters has been fitted separately to a split function of φ. The split functions consist of two parts; the first part holds for the sites with $0^o < \varphi \leq 23.6^o$N and the second part of $21^o < \varphi < 71^o$N. The second part was started from 21°N in order to bridge the region around $\varphi = 21^o$-23.6^o and result to a smooth continuous fitting taking into account those two different fitting functions. This approach provides a better prediction for H(n) in the transition geographical region.

The required general expressions for the parameters A_1, B_1, B_2, C_1, C_2, D_1 and D_2 are given in eqs. (5)-(11) and are based for the first part (tropical region) with $0^o < \varphi \leq 21^o$N on a series of three to eight Gaussian functions with φ (in degrees) as argument, while the second part which represents regions with $21^o < \varphi < 71^o$N is composed by a series of exponential functions. In the case of the parameters B_1 and B_2, the second part of the split function for $21^o<\varphi<71^o$ is expressed by the product of an exponential term with a cosine function. In the transition region, $21^o < \varphi \leq 23.6^o$N, as earlier mentioned, the parameters are giving better results on taking the average of both functions. The values of the parameters a_i, b_i, c_i, which appear in the Gaussian functions, are given in Table 2. The regression analysis followed determined the number of Gaussian terms which provided the best fit. The values of a_i, b_i and c_i, differ for each parameter, A_1, B_1, B_2, C_1, C_2, D_1, D_2. The fitting results for the parameters A_1, B_1, B_2, C_1, C_2, D_1, D_2 along with their coefficient of determination R^2 are shown in Figs. 5-11.

$$A_1 = \begin{cases} \sum_{i=1}^{3} a_i \, exp\left[-\left(\frac{\varphi - b_i}{c_i}\right)^2\right], & 0^o < \varphi \leq 23.6°N \\ 12.680 \cdot \exp\left(-1.523 \cdot \varphi \frac{\pi}{180}\right) - 15.820 \cdot \exp\left(-5.918 \cdot \varphi \frac{\pi}{180}\right), & 21^o < \varphi < 71°N \end{cases} \quad (5)$$

$$B_1 = \begin{cases} \sum_{i=1}^{8} a_i \, exp\left[-\left(\frac{\varphi - b_i}{c_i}\right)^2\right], & 0^o < \varphi \leq 23.6°N \\ -5.336 \cdot \exp\left(-1.270 \cdot \varphi \frac{\pi}{180}\right) \cdot \cos\left(1.373 \cdot \varphi \frac{\pi}{180} - 1.795\right), & 21^o < \varphi < 71°N \end{cases} \quad (6)$$

$$B_2 = \begin{cases} \sum_{i=1}^{4} a_i \, exp\left[-\left(\frac{\varphi - b_i}{c_i}\right)^2\right], & 0^o < \varphi \leq 23.6°N \\ -3.744 \cdot \exp\left(-0.978 \cdot \varphi \frac{\pi}{180}\right) \cdot \cos\left(-1.587 \cdot \varphi \frac{\pi}{180} + 1.837\right), & 21^o < \varphi < 71°N \end{cases} \quad (7)$$

$$C_1 = \begin{cases} \sum_{i=1}^{6} a_i \, exp\left[-\left(\frac{\varphi - b_i}{c_i}\right)^2\right], & 0^o < \varphi \leq 23.6°N \\ 3.370E-10 \cdot \exp\left(15.030 \cdot \varphi \frac{\pi}{180}\right) + 0.718 \cdot \exp\left(0.465 \cdot \varphi \frac{\pi}{180}\right), & 21^o < \varphi < 71°N \end{cases} \quad (8)$$

$$C_2 = \begin{cases} \sum_{i=1}^{6} a_i \, exp\left[-\left(\frac{\varphi - b_i}{c_i}\right)^2\right], & 0^o < \varphi \leq 23.6°N \\ 1.434E14 \cdot \exp\left(-88.640 \cdot \varphi \frac{\pi}{180}\right) + 0.639 \cdot \exp\left(0.589 \cdot \varphi \frac{\pi}{180}\right), & 21^o < \varphi < 71°N \end{cases} \quad (9)$$

$$D_1 = \begin{cases} \sum_{i=1}^{3} a_i \, exp\left[-\left(\frac{\varphi - b_i}{c_i}\right)^2\right], & 0^o < \varphi \leq 23.6°N \\ -0.002 \cdot \exp\left(4.848 \cdot \varphi \frac{\pi}{180}\right) + 32.600 \cdot \exp\left(-8.874 \cdot \varphi \frac{\pi}{180}\right), & 21^o < \varphi < 71°N \end{cases} \quad (10)$$

$$D_2 = \begin{cases} \sum_{i=1}^{6} a_i \, exp\left[-\left(\frac{\varphi - b_i}{c_i}\right)^2\right], & 0^o < \varphi \leq 23.6°N \\ -0.029 \cdot \exp\left(2.715 \cdot \varphi \frac{\pi}{180}\right) + 0.857 \cdot \exp\left(-1.579 \cdot \varphi \frac{\pi}{180}\right), & 21^o < \varphi < 71°N \end{cases} \quad (11)$$

For the overlapping region $21^o < \varphi \leq 23.6^o$N it is suggested that the average of the two functions is used as it provides better estimates. For sites with latitude $|\varphi| \leq 0.08$, the values of B_1 and B_2 are set equal to 2.5.

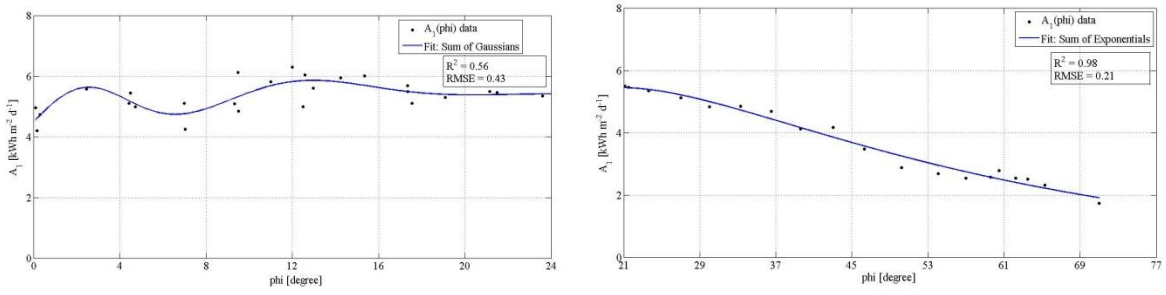

(a) (b)

Fig. 5: Parameter A_1, (a) Gaussian Fitting with 3 terms for latitudes $0^o<\varphi \leq 23.6^oN$, and (b) exponential fitting with 2 terms for latitudes $21^o<\varphi<71^oN$.

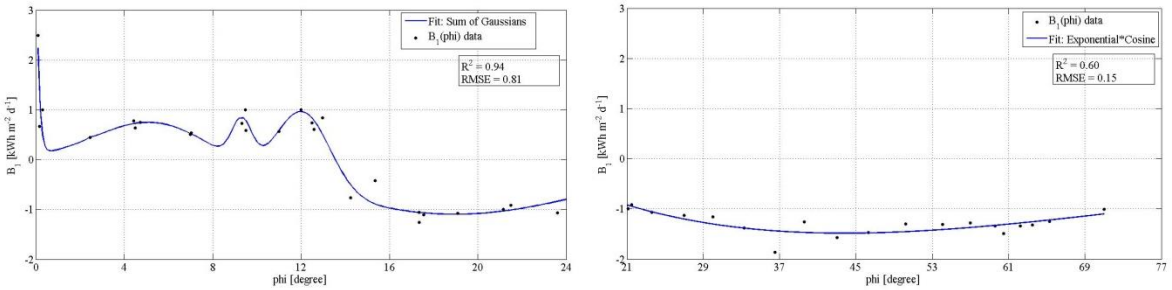

(a) (b)

Fig. 6: Parameter B_1, (a) Gaussian Fitting with 8 terms for latitudes $0^o< \varphi \leq 23.6^oN$, and (b) exponential-cosine fitting for latitudes $21^o< \varphi <71^oN$.

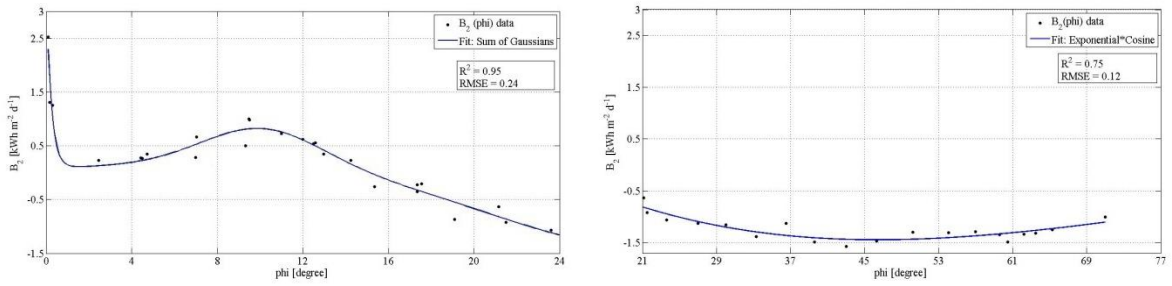

(a) (b)

Fig. 7: Parameter B_2, (a) Gaussian Fitting with 4 terms for latitudes $0^o< \varphi \leq 23.6^oN$, and (b) exponential-cosine fitting for latitudes $21^o< \varphi <71^oN$.

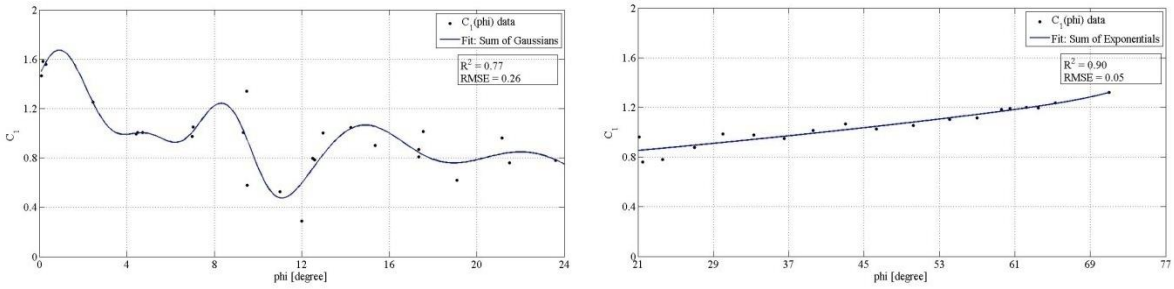

(a) (b)

Fig. 8: Parameter C_1, (a) Gaussian Fitting with 6 terms for latitudes $0^o< \varphi \leq 23.6^oN$, and (b) exponential fitting with 2 terms for latitudes $21^o< \varphi <71^oN$.

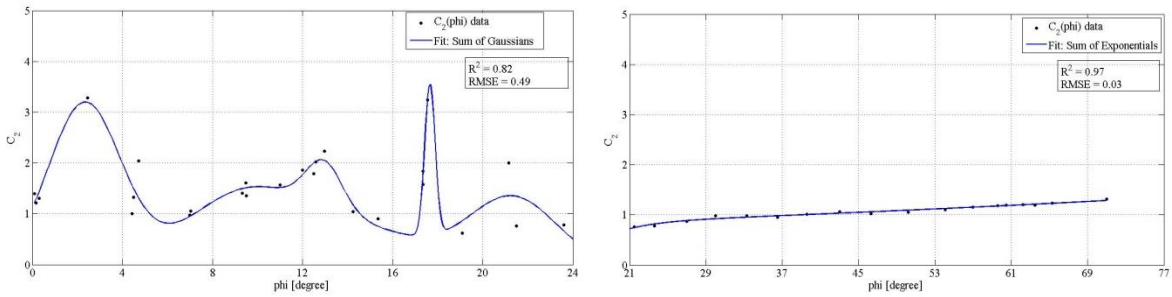

(a) (b)

Fig. 9: Parameter C_2, (a) Gaussian Fitting with 6 terms for latitudes $0^o < \varphi \leq 23.6^o N$, and (b) exponential fitting with 2 terms for latitudes $21^o < \varphi < 71^o N$.

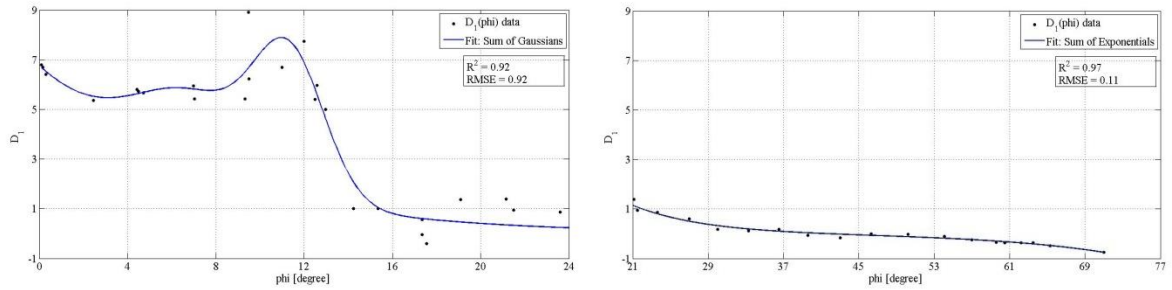

(a) (b)

Fig. 10: Parameter D_1, (a) Gaussian Fitting with 3 terms for latitudes $0^o < \varphi \leq 23.6^o N$, and (b) exponential fitting with 2 terms for latitudes $21^o < \varphi < 71^o N$.

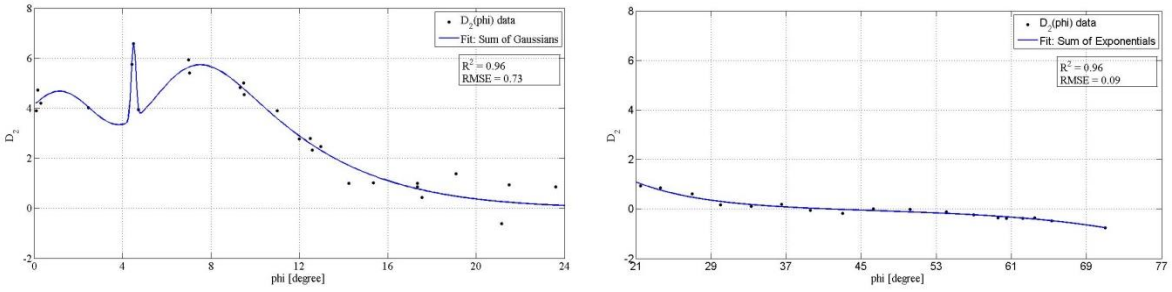

(a) (b)

Fig. 11: Parameter D_2, (a) Gaussian Fitting with 6 terms for latitudes $0^o < \varphi \leq 23.6^o N$, and (b) exponential fitting with 2 terms for latitudes $21^o < \varphi < 71^o N$.

Table 2: Parametric values of the Gaussian functions associated with A_1, B_1, B_2, C_1, C_2, D_1, D_2.

	Model Parameter						
Parameter of the Gaussian Functions	A_1	B_1	B_2	C_1	C_2	D_1	D_2
$\mathbf{a_1}$	1.290	7.790E14	8.17E14	-7.599	3.165	3.156	3.258
$\mathbf{b_1}$	11.600	-7.270	-16.020	2.859	2.326	7.031	4.510
$\mathbf{c_1}$	5.275	1.273	2.783	2.549	2.274	3.876	0.155
$\mathbf{a_2}$	5.417	1.373	-2.063	0.408	2.935	5.458	0.000
$\mathbf{b_2}$	24.880	12.14	28.240	9.419	17.650	11.350	10.000
$\mathbf{c_2}$	30.570	1.560	11.680	1.320	0.322	2.256	0.160
$\mathbf{a_3}$	2.432	-3.713E4	0.697	8.735	0.919	4.78E15	0.000
$\mathbf{b_3}$	2.089	9.275	10.060	2.727	12.960	-500.200	8.326
$\mathbf{c_3}$	3.425	0.016	3.916	2.905	1.145	85.530	0.170
$\mathbf{a_4}$		0.829	0.661	0.943	1.308		-6.491
$\mathbf{b_4}$		5.670	26.570	14.470	21.320		3.933
$\mathbf{c_4}$		3.690	18.800	3.421	2.733		2.696
$\mathbf{a_5}$		-1.126		0.897	0.717		-18.510
$\mathbf{b_5}$		19.500		8.118	13.910		-2.190
$\mathbf{c_5}$		7.739		1.529	4.459		4.356
$\mathbf{a_6}$		0.788		0.841	1.246		28.220
$\mathbf{b_6}$		9.157		22.170	9.284		-8.559
$\mathbf{c_6}$		0.743		5.405	3.636		13.620
$\mathbf{a_7}$		-0.169					
$\mathbf{b_7}$		7.405					
$\mathbf{c_7}$		0.693					
$\mathbf{a_8}$		0.065					
$\mathbf{b_8}$		2.450					
$\mathbf{c_8}$		0.263					

4. Validation of the Model

The model defined by eq.(4) and the mathematical parametric expressions in eqs. (5)-(11) were validated by choosing 8 sites from the Northern and 4 sites from the Southern Hemispheres, including both the tropical and temperate zones extended to the Eastern and Western Hemispheres. These sites are listed below and are separate from the set of sites used for model training in Table 1.

Selected sites in the Northern Hemisphere:

1. Kampala, Uganda (0.19^{o}N, 32.37^{o}E)
2. Singapore (1.22^{o}N, 103.59^{o}E)

3. Addis Abeba, Ethiopia (9.03°N, 38.75°E)
4. Matam, Senegal (15.65°N, 13.25°E)
5. New Delhi, India (28.35°N, 77.12°E)
6. Almeria, Spain (36.85°N, 2.38°W)
7. New York, USA (40.46°N, 73.54°W)
8. Helsinki, Finland (60.19°N, 24.58°E)

Selected sites in the Southern Hemisphere:

1. Lichinga, Mozambique (13.28°S, 35.25°E)
2. Harare, Zimbabwe (17.5°S, 31.01°E)
3. Pretoria, South Africa (25.45°S, 28.14°E)
4. Perth, Australia (31.57°S, 115.52°E)

The mean monthly daily global horizontal solar radiation values as determined by the proposed model for each of the sites in the Northern Hemisphere are compared to the corresponding values for the sites given by the SoDa and NASA databases, in Figs.12(a)-(h). A comparison with the actual measured values for the same sites at ground stations as provided by Meteonorm database is also shown. This proves that the predicted H(n) values are close to the measured data and are not tied to a specific database. As it concerns the validation of the model for the Southern Hemisphere, the comparison followed the same procedure as for the Northern one. The results are shown in Figs.13(a)-(d). Parameters D_1 and D_2 in the model, eq.(4), are phase shifts. For the Southern Hemisphere the estimated parameters D_1 and D_2 are increased by π.

Qualitatively, the graphs in Fig.12 for most cities show that the model provides similar profile as that of the measured data. It does not succeed so well at the sites of Kampala, Uganda (Fig.12(a)) and New Delhi, India (Fig.12(e)), this may be due to the microclimate of the region, which is clear as the data in Figs. 5-11 for $\varphi<23^o$ show considerable scatter along the fitting curve. In the sites of the Southern Hemisphere, as shown in Fig.13, the proposed model provides a prediction of similar profile with the measured data, although larger deviations are observed (e.g. Fig.13(a)).

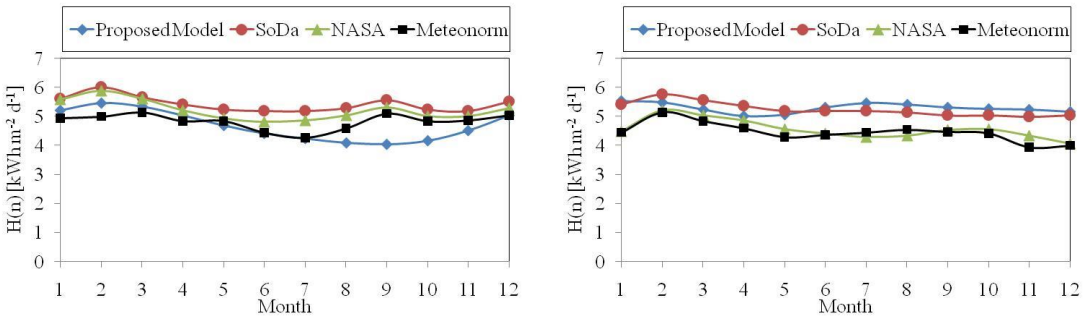

(a) (b)

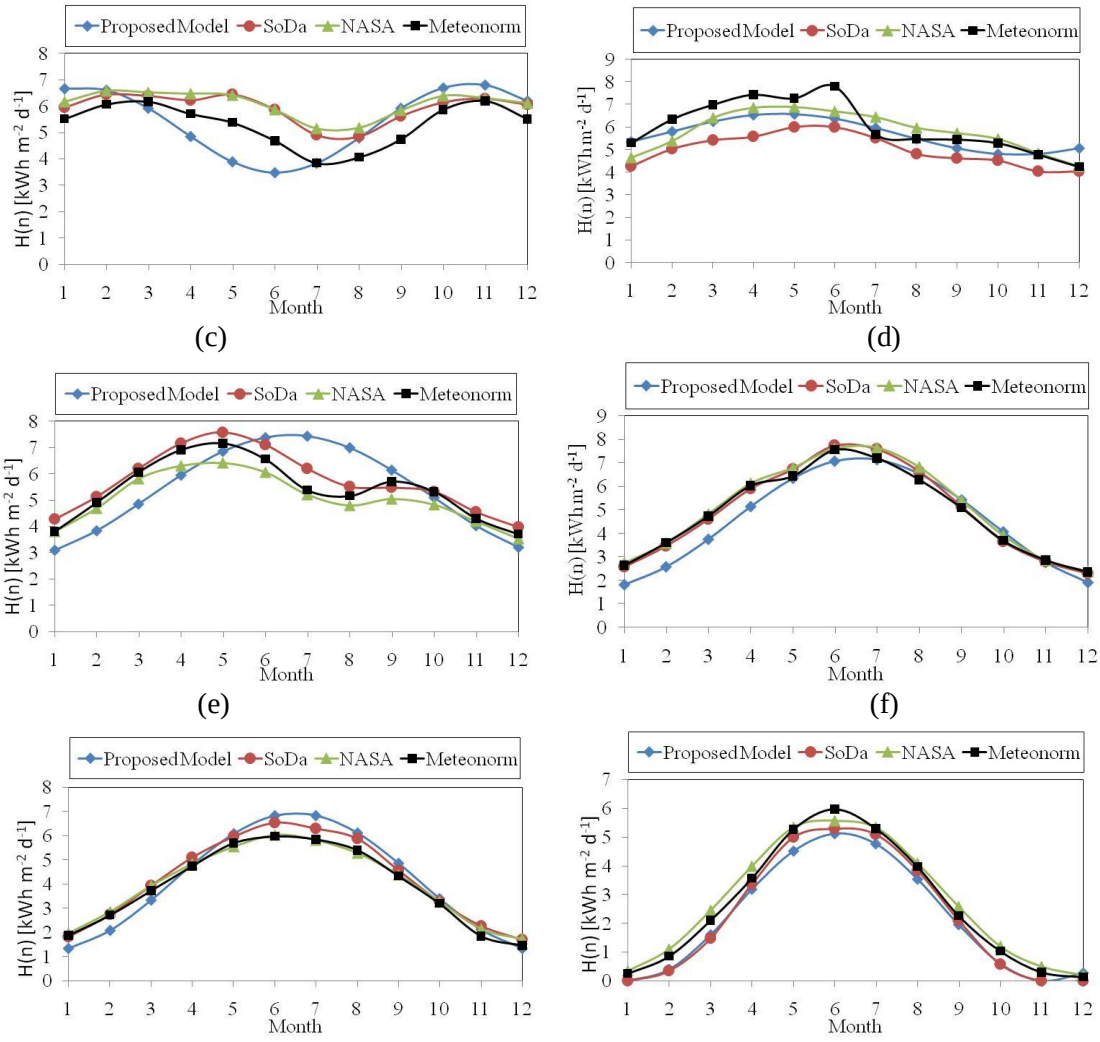

Fig. 12: H(n) predicted by the proposed model in comparison to the mean monthly daily H(n) data provided by SoDa, NASA and Meteonorm databases, for the cities of the Northern Hemisphere (a) Kampala, Uganda, (b) Singapore, (c) Addis Abeba, Ethiopia, (d) Matam, Senegal, (e) New Delhi, India, (f) Almeria, Spain, (g) New York, USA, (h) Helsinki, Finland.

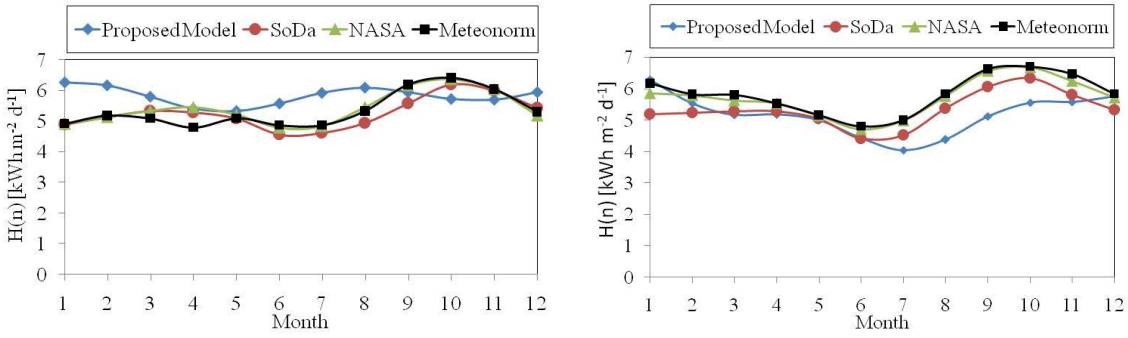

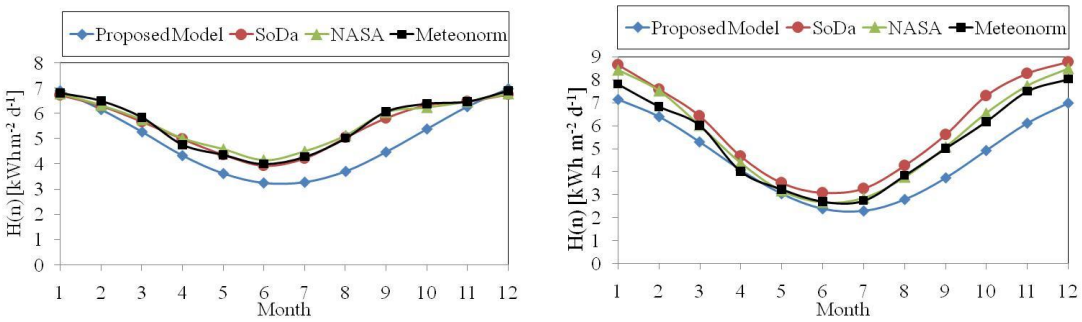

Fig. 13: As in Fig.12, but for the cities of the Southern Hemisphere (a) Lichinga, Mozambique, (b) Harare, Zimbabwe, (c) Pretoria, SA, (d) Perth, Australia.

Statistical results of the Normalised Mean Bias Error (NMBE), the Normalised Root Mean Square Error (NRMSE) and t statistic, eqs. (12)-(14), are given for comparison of the predicted H(n) values by the proposed model for each month with the H(n) values of NASA, SoDa and Meteonorm databases for the above cities in Table 3.

$$MBE = \frac{1}{N}\sum_{i=1}^{N}(e_i - m_i), \qquad NMBE = \frac{\frac{1}{N}\sum_{i=1}^{N}(e_i - m_i)}{\frac{1}{N}\sum_{i=1}^{N}(m_i)} \tag{12}$$

$$RMSE = \sqrt{\frac{1}{N}\sum_{i=1}^{N}(e_i - m_i)^2}, \qquad NRMSE = \frac{\sqrt{\frac{1}{N}\sum_{i=1}^{N}(e_i - m_i)^2}}{\frac{1}{N}\sum_{i=1}^{N}(m_i)} \tag{13}$$

$$t = \sqrt{\frac{(N-1)MBE^2}{RMSE^2 - MBE^2}} \tag{14}$$

where e_i is the ith estimated value by the proposed model and m_i is the ith measured value. Here, i is the month and N the number of months (N=12).

As shown in Table 3, the NMBE statistic is negative for the comparison of the model with the SoDa database for all cities except three, where it underestimates the H(n) value by less than 14% in 8 out of 9 cities, and overestimates by up to 14% in the remaining 3. The corresponding comparison with NASA database shows a mixed behavior of overestimation and underestimation, with absolute values considerably less than 12% with the exception of Singapore having NMBE of 16%, Helsinki of -20.7% and Perth of -17.3%. The NRMSE is generally lower than 16% for both databases. However, NRMSE in the case of New Delhi takes a value of 22.2% for NASA and 17.6% for SoDa, Helsinki 22.6% and 9.8% and Perth 19.8% and 24.8%, respectively. The comparison of the model with the measured values provided by Meteonorm, show a similar underestimation of H(n) with NMBE of generally less than 15% and NRMSE below 20%. The larger deviations occur in the same cities as mentioned previously.

Considering the t-test for comparing the predicted H(n) values by the proposed model with the values provided by the two databases, the absolute value of this statistic was less than the critical value, suggesting that the result is significant, in all but three cities in the Northern Hemisphere for the NASA and the SoDa database. The cities Kampala, Matam and Almeria, where the t values were large for the SoDa database, had low NMBE and NRMSE values.

For the Southern Hemisphere the t-statistic results comparing the model values with the NASA and Meteonorm data were poorer showing a relative insignificance in all 4 cities; this occurred in 3 out of 4 cities for the SoDa database. However, the NMBE and NRMSE corresponding values are lower than 15% in all cases except Perth. It is noteworthy to underline that the regression analysis carried out for the extraction of the parameters of the model was based only on data from the Northern Hemisphere. However, even for the Southern Hemisphere the predicted H(n) profiles are qualitatively in agreement with the measured values.

Table 3: NMBE, NRMSE and t statistic results of the estimated values from the proposed H(n) model in comparison to the corresponding H(n) values of NASA, SoDa and Meteonorm databases for the various cities.

	NASA			**SoDa**			**Meteonorm**		
	NMBE	**NRMSE**	**t**	**NMBE**	**NRMSE**	**t**	**NMBE**	**NRMSE**	**t**
Kampala, Uganda	-0.101	0.118	-5.507	-0.136	0.151	-6.926	-0.028	0.091	-1.063
Singapore	0.160	0.179	6.732	0.009	0.047	0.674	0.187	0.199	9.274
Addis Abeba, Ethiopia	-0.101	0.199	-1.947	-0.077	0.199	-1.385	0.031	0.169	0.621
Matam, Senegal	-0.022	0.086	-0.880	0.139	0.148	9.309	-0.054	0.110	-1.865
New Delhi, India	0.069	0.222	1.263	-0.053	0.176	-0.832	-0.002	0.191	-0.030
Almeria, Spain	-0.101	0.128	-4.255	-0.077	0.115	-2.976	-0.067	0.121	-2.207
New York, USA	0.028	0.152	0.689	-0.018	0.094	-0.475	0.051	0.141	1.281
Helsinki, Finland	-0.207	0.226	-7.823	-0.043	0.098	-1.411	-0.164	0.187	-5.945
Lichinga, Mozambique	0.078	0.136	2.308	0.110	0.156	3.270	0.091	0.143	2.745
Harare, Zimbwawe	-0.095	0.136	-3.304	-0.028	0.112	-0.703	-0.111	0.142	-4.105
Pretoria, SA	-0.120	0.155	-4.034	-0.104	0.138	-3.826	-0.115	0.146	-4.240
Perth, AUS	-0.173	0.198	-6.038	-0.227	0.248	-7.511	-0.136	0.161	-5.232
t(critical at a=0.05) : 2.201									

5. Discussion

The predicted H(n) values are well accepted as they present the solar radiation profile of the 2 peaks for sites with latitude $\varphi<23^{o}$, while for $\varphi> 23^{o}$ the profile provided by the model has one

peak as determined, too, by the one-cosine model, eq.(1). The parameterization of the H(n) model as proposed and outlined in the previous sections was proven to satisfy well a very large geographical area ($0^o<|\varphi|<71^o$) and longitudes along the Eastern to Western Hemispheres. A very important behavior of this model is that it complies with the model of the one cosine [20], as the parameters of the eq.(4) model become $B_1=B_2$, $C_1=C_2\cong 1$ and $D_1=D_2\cong 0$ for $23^o<\varphi<60^o$.

On the other hand, instead of the Gaussian functions, another version of the parametric functions was also tried in the regression analysis, which also gave very promising results. That was based on a series of Fourier harmonics of the following form:

$$B_1 = a_0 + \sum_{s=1}^{k} a_s \cdot \cos\left(\frac{2\pi}{360}\cdot 4\cdot s\cdot \varphi\right) + \sum_{s=1}^{k} b_s \cdot \sin\left(\frac{2\pi}{360}\cdot 4\cdot s\cdot \varphi\right) \quad (15)$$

$$B_2 = a_0 + \sum_{s=1}^{k} a_s \cdot \cos\left(\frac{2\pi}{360}\cdot 4\cdot s\cdot \varphi\right) + \sum_{s=1}^{k} b_s \cdot \sin\left(\frac{2\pi}{360}\cdot 4\cdot s\cdot \varphi\right) \quad (16)$$

$$D_1 = a_0 + \sum_{s=1}^{k} a_s \cdot \cos\left(\frac{2\pi}{360}\cdot 4\cdot s\cdot \varphi\right) + \sum_{s=1}^{k} b_s \cdot \sin\left(\frac{2\pi}{360}\cdot 4\cdot s\cdot \varphi\right) \quad (17)$$

$$D_2 = a_0 + \sum_{s=1}^{k} a_s \cdot \cos\left(\frac{2\pi}{360}\cdot 4\cdot s\cdot \varphi\right) + \sum_{s=1}^{k} b_s \cdot \sin\left(\frac{2\pi}{360}\cdot 4\cdot s\cdot \varphi\right) \quad (18)$$

In the above Fourier functions, *s* takes values from 1 to 4-8.

In the first attempt eqs. (15)-(18) were applied in the regression analysis for the whole area of latitudes $0^o< |\varphi|<71^o$.

In another attempt of the regression analysis the above Fourier functions replaced the Gaussian functions in the proposed model for latitudes $0^o<\varphi<23^o$, while the exponential functions, eqs.(5)-(11), were used for the rest of the latitudes $23^o<\varphi<71^o$.

The results with both modes of Fourier functions were of the same quality and similar predictive capacity in comparison to the proposed model based on Gaussians, as it concerns H(n). The comparison of the proposed model with the above two versions of the Fourier expansion of the parametric functions A-D will be presented in a next paper.

6. Conclusions

This paper outlines a generalized model to predict the mean expected daily global solar radiation H(n) on the horizontal plane for any site of latitude φ, on any day, n. The model is based on a two-cosine function while the seven parameters A_1, B_1, B_2, C_1, C_2, D_1, D_2 in the model are determined through a series of Gaussian functions for the region of the tropical zones, $0^o<|\varphi|<23^o$, while for the temperate zone and beyond, $23^0<|\varphi|<71^0$ the values of the parameters are determined from a series of exponential functions or in the case of the parameters B_1 and B_2 from a product of an exponential function with a cosine function. The model was validated by

taking at random 12 sites to predict H(n), eight in the Northern and four in the Southern Hemispheres. Those sites were different from the 42 sites used for the model training and whose H(n) values were obtained from SoDa database. For the model validation the predicted H(n) values were compared also with the values from the NASA database and the measured values at those sites provided by the Meteonorm database. The validation was based on three statistical criteria, the NMBE, NRMSE and t-statistic. For most of the cities of the Northern and Southern Hemisphere and for the Eastern and Western Hemispheres the NMBE and NRMSE values were less than 15%. Only for Perth the three statistical criteria gave poor results for the three databases. It should be noted that similar statistical results were produced when comparing values from NASA or SoDa database to the measured values of Meteonorm database.

The proposed model succeeds for most latitudes from 0^o to 71^o in the Northern and Southern Hemispheres and most longitudes in the East and West. This universal model requires only the number of the day n and the latitude φ, which underlines its utilizability especially in places that no meteorological data are available. Thus, the proposed model exceeds previous models such as eqs. (1)-(3) which rely on the analysis of solar radiation data for each region, while eq.(1) is valid for limited range of latitudes. Finally, the proposed model in comparison to any other may be easily integrated into sizing or simulation algorithms relevant to PV, solar collectors and similar applications.

References

1.Iqbal M. An Introduction to solar radiation. Toronto: Academic Press; 1983

2.ASHRAE handbook: HVAC applications, Atlanta (GA): ASHRAE; 1999

3.Wong LT, Chow WK. Solar radiation model. Applied Energy 2001;69:191-224.

4.Angström A. Solar and terrestrial radiation. Quart. J. Roy. Met. Soc. 1924;50:121-5.

5.Cotfas DT, Cotfas PA, Kaplani E, Samoila C. Monthly average daily global and diffuse solar radiation based on sunshine duration and clearness index for Brasov, Romania. Journal of Renewable and Sustainable Energy 2014;6:053106.

6.Ahmad Jamil M, Tiwari GN. Solar radiation models-review. International Journal of Energy and Environment 2010;1(3):513-32.

7.El-Sebaii AA, Al-Hazmi FS, Al-Ghamdi AA, Yaghmour SJ. Global, direct and diffuse solar radiation on horizontal and tilted surfaces in Jeddah, Saudi Arabia. Applied Energy 2010;87(2):568-76.

8. Jin Z, Yezheng W, Gang Y. General formula for estimation of monthly average daily global solar radiation in China. Energy Conversion and Management 2005;46(2):257-68.

9.Namrata K, Sharma SP, Saksena SBL. Comparison of different models for estimation of global solar radiation in Jharkhand (India) Region. Smart Grid and Renewable Energy 2013;4(4):348-52.

10. Ahmad F, Ulfat I. Empirical models for the correlation of monthly average daily global solar radiation with hours of sunshine on a horizontal surface at Karachi, Pakistan. Turk J Phys 2004; 28:301-7.

11. Muneer T, Gul M, Kambezidis HD. Evaluation of an all-sky meteorological radiation model against long-term measured hourly data. Energy Conv. Manage. 1998;39(3-4):303-317.

12. Psiloglou BE, Kambezidis HD. Performance of the meteorological radiation model during the solar eclipse of 29 March 2006. Atmos. Chem. Phys. 2007;7(23):6047-6059.

13. Besharat F, Dehghan AA, Faghih AR. Empirical models for estimating global solar radiation: A review and case study. Renewable and Sustainable Energy Reviews 2013;21:798-821.

14.Almorox J, Hontoria C. Global solar radiation estimation using sunshine duration in Spain. Energy Conversion and Management 2004;45:1529-35.

15.El-Metwally M. Sunshine and global solar radiation estimation at different sites in Egypt. Journal of Atmospheric and Solar –Terrestrial Physics 2005;67(14):1331-42.

16.Paltridge GW, Proctor D. Monthly mean solar radiation statistics in Australia. Solar Energy 1976;18(3):235-43.

17.Mellit A, Kalogirou SA, Shaari S,Salhi H, Hadj Arab A. Methodology for predicting sequences of mean monthly clearness index and daily solar radiation data in remote areas: Application of sizing a stand-alone PV system. Renewable Energy Vol.33(2008)pp1570-1590

18.Li H, Ma W, Lian Y, Wang X. Estimating daily global solar radiation by day of the year in China. Applied Energy 2010;87(10):3011-7.

19.Khorasanizadeh H, Mohammadi K, Jalilvand M. A statistical comparative study to demonstrate the merit of day of the year-based models for estimation of horizontal global solar radiation. Energy Conversion and management 2014;87:37-47.

20. Kaplanis S, Kaplani E. A model to predict expected mean and stochastic hourly global solar radiation $I(h,n_j)$ values. Renewable Energy 2007;32:1414-25.

21. Korachagaon I, Bapat VN. General formula for the estimation of global solar radiation on earth`s surface around the globe. Renewable Energy 2012;41:394-400.

22. Li H, Cao F, Bu X, Zhao L. Models for calculating daily global solar radiation from air temperature in humid regions-A case study. Environmental Progress and Sustainable Energy 2015;34(2):595-9.

23. Ajayi OO, Ohijeagbon OD, Nwadialo CE, Olumide Olasope. New model to estimate daily global solar radiation over Nigeria. Sustainable Energy Technologies and Assessments 2014;5:28-36.

24. Kaplani E, Kaplanis S. Prediction of solar radiation intensity for cost-effective PV sizing and intelligent energy buildings. In book Solar Power, Radu Rugescu (Ed.), ISBN:978-953-51-0014-0, Croatia: Intech; 2012.

25. Joint Research Centre, Institute for Energy and Transport. Photovoltaic Geographical Information System (PVGIS). http://re.jrc.ec.europa.eu/pvgis/

26. Solar radiation data (SoDa). http://www.soda-is.com

27. Meteonorm Software. http://meteonorm.com/

28. NREL. PVWatts Calculator. http://pvwatts.nrel.gov/

29. NREL. National Solar Radiation Data Base. http://rredc.nrel.gov/solar/old_data/nsrdb/

30. NASA. Surface meteorology and solar energy. A renewable energy resource web site (release 6.0). https://eosweb.larc.nasa.gov/sse/

31. Natural Resources Canada. RETScreen International. http://www.retscreen.net/

32. Collares-Pereira M, Rabl A. The average distribution of solar radiation-correlations between diffuse and hemispherical and between daily and hourly insolation values. Solar Energy 1979;22(2):155-64.

33. Gueymard C. Prediction and performance assessment of mean hourly global radiation. Solar Energy 2000; 68(3):285-303.

34. Baig A, Akhter P, Mufti A. A novel approach to estimate the clear day global radiation. Renewable Energy 1991;1(1):119-123.

35. Kaplanis S. New methodologies to estimate the hourly global solar radiation; Comparisons with existing models. Renewable Energy 2006;31:781-90.